J. Fluid Mech. (2006), *vol.* 551, *pp.* 117–139.
doi:10.1017/S0022112005008396 Printed in the United Kingdom

Bifurcation and stability analysis of laminar isothermal counterflowing jets

By R. P. PAWLOWSKI[1,2]†, A. G. SALINGER[2]
J. N. SHADID[2] AND T. J. MOUNTZIARIS[1]‡

[1]SUNY at Buffalo, Department of Chemical Engineering, Buffalo, NY 14260, USA
[2]Sandia National Laboratories, Albuquerque, NM 87185, USA

(Received 7 September 2004 and in revised form 9 September 2005)

We present a numerical study of the structure and stability of laminar isothermal flows formed by two counterflowing jets of an incompressible Newtonian fluid. We demonstrate that symmetric counterflowing jets with identical mass flow rates exhibit multiple steady states and, in certain cases, time-dependent (periodic) steady states. Two geometric configurations were studied based on the inlet jet shapes: planar and axisymmetric. Stagnation flows formed by planar counterflowing jets exhibit both steady-state multiplicity and time-dependent behaviour, while axisymmetric jets exhibit only a steady-state multiplicity. A linearized bifurcation and stability analysis based on the continuity and Navier–Stokes equations revealed transitions between a single (symmetric) steady state and multiple steady states or periodic steady states. The dimensionless quantities forming the parameter space of this system are the inlet Reynolds number (Re) and a geometric aspect ratio (α), equal to the jet inlet characteristic length (used for calculating Re) divided by the jet separation. The boundaries separating different flow regimes have been identified in the (Re, α) parameter space. The resulting flow maps are useful for the design and operation of counterflow jet reactors.

1. Introduction

Stagnation flows formed by symmetric counterflowing jets have been used in a wide variety of applications including kinetic studies of diffusion flames (Puri *et al.* 1987; Zhao & Isaac 1997), polymer processing (Wood *et al.* 1991), nanoparticle synthesis (Zachariah & Semerjian 1989; Sarigiannis *et al.* 2002), studies of blood flow (Grimes *et al.* 1996), and kinetic studies in a wall-less environment (Safvi & Mountziaris 1993; Safvi 1995; Gupta, Safvi & Mountziaris 1996). A comprehensive discussion on counterflowing jet reactor applications can be found in Tamir (1994). Understanding the structure and stability of such flows is critical for controlling the operating conditions of processing equipment that lead to desirable results.

Instabilities in counterflowing jets can be generated either thermally or hydrodynamically. The bifurcation analysis of thermal instabilities has been a subject of intense study in the combustion community. Much of the work has centred on tracking solution branches to find ignition and extinction points (turning points)

† Author to whom correspondence should be addressed: rppawlo@sandia.gov
‡ Current Address: Department of Chemical Engineering, University of Massachusetts, Amherst, MA 01003, USA.

of the diffusion flames and identifying how operating conditions can affect these characteristic points in parameter space (Liñán 1974, Vlachos, Schmidt & Aris 1993; Fotache, Kreutz & Law 1997). Non-isothermal counterflowing jets can also exhibit instabilities without combustion, just by heating one of the jets and keeping the other jet cool. Experiments have shown that when counterflowing jets are aligned vertically, chaotic flows can develop if only the lower jet is heated (Pawlowski 2000).

Hydrodynamic instabilities in isothermal flows formed by counterflowing jets have attracted less attention. Reported experimental observations suggest that even when the mass flow rates of the two streams are equal, the resulting flows may still exhibit multiple steady states or oscillatory behaviour (Rolon, Veynante & Martin 1991; Denshchikov, Kontratev & Romashev 1978; Denshchikov *et al.* 1983). Such unexpected phenomena can have detrimental effects on research and industrial applications employing such flows by affecting the reproducibility and interpretation of the results. In order to successfully exploit counterflowing jets for practical applications, it is important to identify the critical parameter values corresponding to transitions from a single steady state to multiple ones or to oscillatory behaviour.

Rolon *et al.* (1991) observed multiple steady states in experiments using isothermal counterflowing streams of air. If the inlet mass flow rates are equal, the stagnation point is expected to be located half-way between the two inlets. Their experimental observations however have shown the existence of two stable steady states, each having a stagnation point on the axis of symmetry, but equally displaced from the centre towards one or the other jet inlet. The two stable flow regimes observed were mirror images and the phenomenon was called 'bi-stability'. These observations indicate the possible existence of a pitchfork bifurcation. The two observed steady states apparently correspond to the stable steady states on the upper and lower branches of the pitchfork, while the middle steady state cannot be realized because it is unstable.

Denshchikov *et al.* (1978, 1983) studied planar (rectangular) counterflowing jets of water under isothermal conditions and observed oscillatory behaviour under certain flow rates and geometric configurations. The oscillatory flow was called a 'deflecting jet oscillation'. In the oscilliatory flow regime each jet was deflected in the opposite direction from the other and they periodically switch directions. These observations suggest the presence of a Hopf bifurcation.

Motivated by the above observations, we performed a bifurcation and linearized stability analysis of laminar flows arising from isothermal counterflowing jets. The use of stability analyses in complex flows at finite Reynolds numbers (Re) was pioneered by L. E. Scriven (Bixler & Scriven 1987; Christodoulou & Scriven 1988; Coyle, Macosko & Scriven 1990; Kistler & Scriven 1994). Our objectives are to: (a) reproduce the reported experimental observations using computer simulations, (b) identify the critical parameter values leading to multiple steady states or oscillatory behaviour, and (c) understand the underlying physical mechanisms that lead to such behaviour. Two flow geometries are considered in our study of counterflowing jets: (i) planar rectangular jets and (ii) axisymmetric cylindrical jets. Two- and three-dimensional computer simulations were performed based on the fundamental continuity and Navier–Stokes equations. Bifurcation tracking and eigenvalue analysis algorithms were employed to identify the characteristic values of Re and the geometric aspect ratio, α, that correspond to transitions between various flow regimes. Flow regime maps are presented in parameter space based on this analysis. Using such parameter maps counterflow jet reactors can be designed and operated to control the different flow modes.

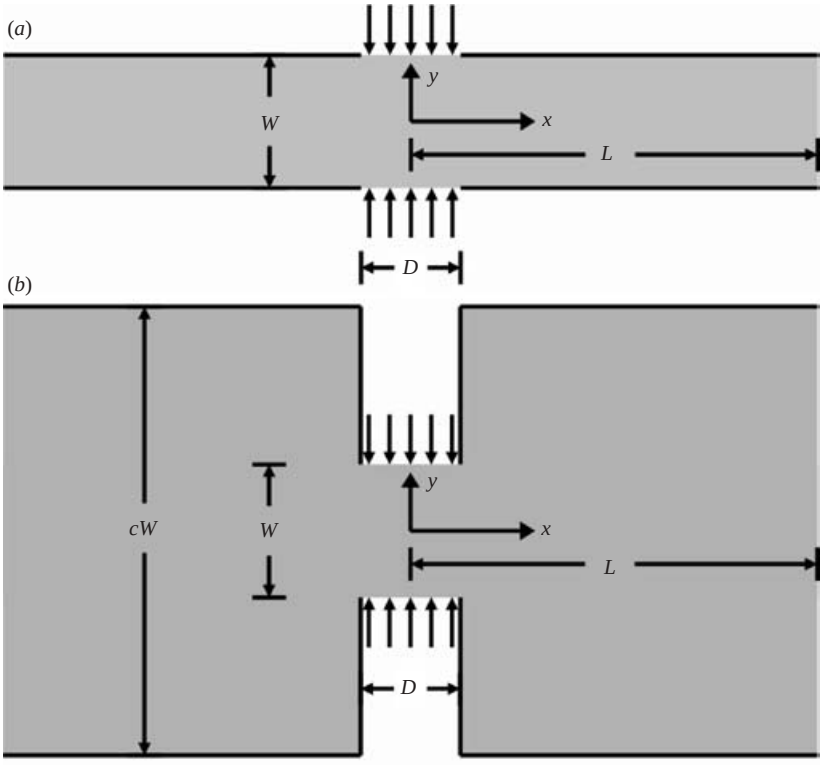

FIGURE 1. (*a*) Planar counterflow jet geometry used in two-dimensional simulations. (*b*) Alternative planar counterflow jet geometry that includes a flow expansion region. Cartesian coordinates are used in both cases.

The remainder of this paper is organized as follows: Section 2 describes the computational models used in our analysis. Section 3 describes the numerical algorithms used to solve the steady-state and transient problems. Finally, the results and conclusions are discussed in § 4 and § 5, respectively.

2. The counterflowing jet model

While analytic solutions for counterflowing jets exist (Leclerc 1950; Bird, Stewart & Lightfoot 1960), it has been shown that such models only capture the flow qualitatively and cannot accurately predict the measured fluid velocities. For a small spacing between the jets, the flow field deviates from these analytic solutions (Rolon *et al.* 1991) and rigorous models, such as those developed by our group (Safvi & Mountziaris 1994), are necessary for accurate prediction of the flow field. The simulation results presented here are based on the fundamental equations describing incompressible fluid flow of a Newtonian fluid in two different geometries.

2.1. *Model geometry*

The geometries used in the analysis are shown in figures 1 and 2. Figure 1(*a*) shows a two-dimensional representation of a *planar* counterflowing jet arrangement with an exit region formed by two parallel horizontal walls aligned with the jet inlets, and the Cartesian coordinate system used in this study. In this case, the characteristic length (used for computing Re) is the width of the inlet, D, the separation between the jets is denoted by W, and the horizontal distance of the exit from the y-axis is L. In the

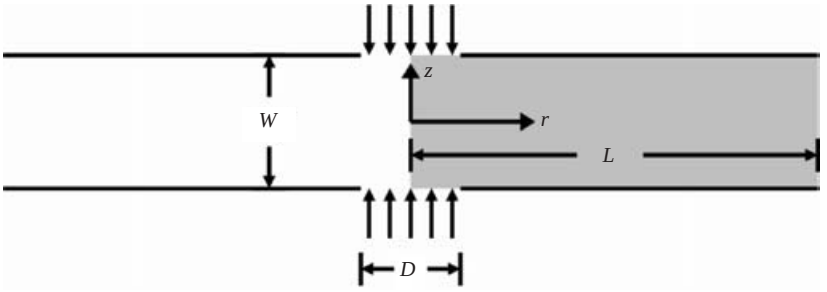

FIGURE 2. Schematic of the geometry used in flow simulations of three-dimensional axisymmetric jets. Cylindrical coordinates are used with a two-dimensional mesh and axial symmetry is assumed. The shaded region corresponds to the discretized (r, z) domain.

simulations the distance L was fixed at ten times the spacing between the jets, W. This was found to be sufficient to eliminate the effects of the exit boundary conditions on the structure of the flow in the stagnation region between the two jets. A variation of this geometry that includes a flow expansion region is shown in figure 1(*b*). This geometry was used in some calculations to test the effect of the walls on the structure of the flow in the stagnation region. In this case the separation of the jet inlets is still W, but the exit region was formed by two horizontal walls positioned at a distance cW from each other, symmetrically on each side of the horizontal midplane, as shown in figure 1(*b*). In our results, c was fixed at a value of 2.0. In both cases, the entire domain indicated by the shaded region is discretized. The two geometries were used to compare our simulations with the work of Denshchikov *et al.* (1978, 1983). An important assumption for the planar jet models is that the flow is always two-dimensional. This means that the third dimension is long enough compared to the other two to allow a two-dimensional flow to develop and that the flow does not become three-dimensional, even when the two-dimensional stagnation flow pattern is disturbed and becomes asymmetric.

To study the structure and stability of stagnation flows formed by *axisymmetric* counterflowing jets, two models were used. The first was based on a three-dimensional axisymetric representation of the flow taken from Gupta *et al.* (1996) and employed cylindrical coordinates (figure 2) on a two-dimensional mesh. The second was a fully three-dimensional model based on Cartesian coordinates that enable the simulation of flows exhibiting a breaking of the axial symmetry (figure 3). A limitation of the simulation code did not allow analysis of three-dimensional disturbances on the two-dimensional axisymmetric mesh. Therefore, the full three-dimensional mesh was required to analyse the complete system.

2.2. *Governing equations*

The governing equations are based on the continuity and Navier-Stokes equations describing laminar isothermal flow of an incompressible Newtonian fluid. The governing partial differential equations (PDEs) are described below in dimensionless form:

total mass conservation

$$\nabla \cdot \boldsymbol{u} = 0; \tag{2.1}$$

momentum conservation

$$\frac{\partial \boldsymbol{u}}{\partial t} + \boldsymbol{u} \cdot \nabla \boldsymbol{u} + \nabla P - \frac{1}{Re} \nabla^2 \boldsymbol{u} = 0. \tag{2.2}$$

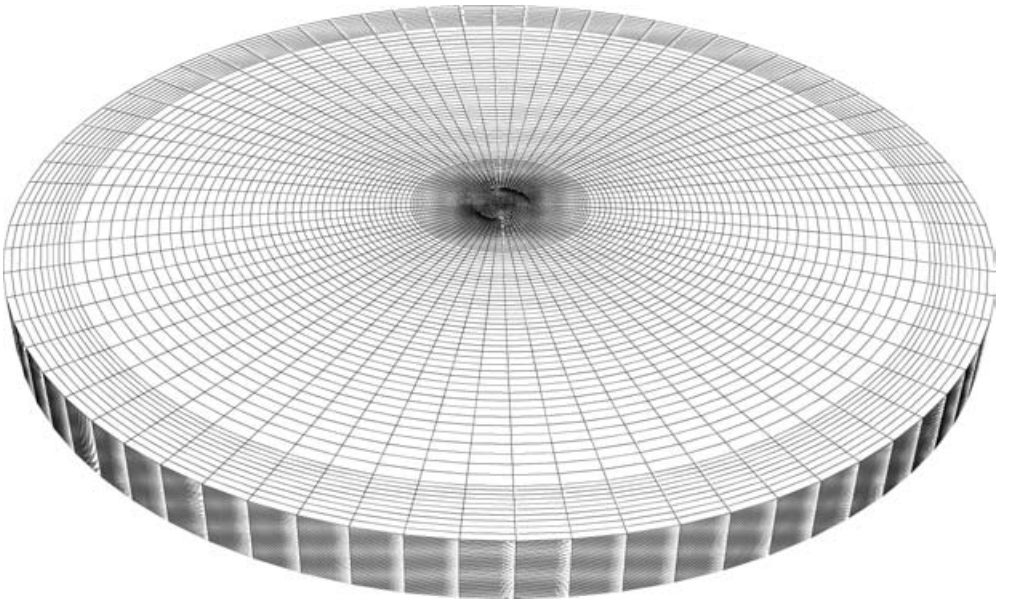

FIGURE 3. Three-dimensional mesh based on a Cartesian coordinate system used to simulate counterflowing jets that may exhibit breaking of symmetry. In the centre, the finite element mesh is unstructured and not axisymmetric.

The unknowns in dimensionless form are $\boldsymbol{u}$, the fluid velocity vector, and P, the dynamic pressure which includes the body force term. Re is the Reynolds number and t is the dimensionless time. We solve a number of momentum equations (equation (2.2)), equal to the number of spatial dimensions.

Equations (2.1) and (2.2) were made dimensionless using a number of characteristic values. Distance was scaled by a characteristic length, D, the inlet jet width or diameter defined in § 2.1. Velocity was scaled by u_o, the inlet velocity of each inlet jet, time was scaled by D/u_o, and pressure was scaled by ρu_o^2. The Reynolds number (Re) in equation (2.2) is defined as

$$Re = \frac{\rho D u_o}{\eta}, \tag{2.3}$$

where ρ is the fluid density and η is the viscosity of the fluid.

Additional dimensionless parameters may appear when the boundary conditions that are necessary to complete the model are written in dimensionless form. For the simulations discussed the following boundary conditions were used: (i) uniform velocity with absolute value of u_o for the two jet inlets (plug flow), (ii) no slip and no penetration along solid walls ($\boldsymbol{u} = \boldsymbol{0}$), and (iii) no normal stress and no vertical velocity at the exit. Given that L has a fixed value equal to $10W$ and that the expansion region of the geometry appearing in Figure 1(b) is fixed at $2W$, the only additional dimensionless parameter that appears in the boundary conditions is the aspect ratio, α, defined as:

$$\alpha = D/W. \tag{2.4}$$

The simulations discussed in this study correspond to a range of Re from 1 to 1500 for planar jets, 1 to 2100 for axisymmetric jets and aspect ratios between 0.05 and 1.0.

It is important to note that both the planar and axisymmetric models exhibit a reflectional symmetry about the midplane. However, we do not force the solutions to have this symmetry since we expect the symmetry to be broken, as observed by Rolon *et al.* (1991).

3. Numerical methods

The numerical methods that are essential for this analysis must allow computation of steady and transient solutions, continuation of a steady-state solution branch as the value of a parameter is changing, computation of the bifurcation points, stability analysis by tracking the leading eigenvalues, and continuation of bifurcation points in parameter space. The code MPSalsa, developed by Sandia National Laboratories (Shadid *et al.* 1996; Salinger *et al.* 1996), is used to discretize and solve the partial differential equations for the steady-state and transient counterflow jet models. MPSalsa is designed to solve laminar, low-Mach-number, two- and three-dimensional incompressible reacting fluid flows on massively parallel computers. The continuation and bifurcation tracking capabilities are provided by the Library of Continuation Algorithms (LOCA), also developed at Sandia (Salinger *et al.* 2002*a*, 2005). Linear systems were solved using the Aztec parallel iterative solver library (Hutchinson, Shadid & Tuminaro 1995). The numerical methods and solution algorithms used for the bifurcation and stability analysis are briefly discussed in the following sections.

3.1. *Discretization of PDEs*

A stabilized-Galerkin finite element formulation is used to spatially discretize equations (2.1) and (2.2). The stabilized method allows equal-order interpolation of velocity and pressure unknowns and also provides stabilization of the convection operators to limit oscillations due to high grid Reynolds number effects. This formulation is based on the work of Hughes, Franca & Balestra (1986) and Tezduyar (1992). Specifically, the discrete equations are obtained from the following residual equations:

momentum

$$F_{\boldsymbol{u}_i} = \int_{\Omega} R_{m_i} \Phi \, \mathrm{d}\Omega + \sum_e \int_{\Omega^e} \tau_m (\boldsymbol{u} \cdot \nabla \Phi) R_{m_i} \, \mathrm{d}\Omega; \tag{3.1}$$

total mass

$$F_P = \int_{\Omega} R_P \Phi \, \mathrm{d}\Omega + \sum_e \int_{\Omega^e} \rho \tau_m \nabla \Phi \cdot \boldsymbol{R_m} \, \mathrm{d}\Omega. \tag{3.2}$$

The Φ are the trial functions corresponding to the Galerkin finite element method and i is the index of the spatial dimension. R_{m_i} and R_P are the residuals corresponding to equations (2.2) and (2.1) respectively:

$$\boldsymbol{R_m} = \frac{\partial \boldsymbol{u}}{\partial t} + \boldsymbol{u} \cdot \nabla \boldsymbol{u} + \nabla P - \frac{1}{Re} \nabla^2 \boldsymbol{u}, \tag{3.3}$$

$$R_P = \nabla \cdot \boldsymbol{u}. \tag{3.4}$$

The final term on the right-hand side of equations (3.1) and (3.2) is the stabilization term. In equation (3.1) this term stabilizes convection and corresponds to SUPG (Streamline Upwind Petrov-Galerkin). The final term in (3.2) stabilizes the velocity–pressure coupling for incompressible flows, allowing equal-order interpolation for the velocity and pressure unknowns. In both stabilization terms τ_m is the stability parameter that is a function of the fluid velocity, $\boldsymbol{u}$, and the dimensionless transport

coefficients appearing in the model. The details of the technique can be found in Hughes *et al.* (1986) and Tezduyar (1992).

The effects of SUPG stabilization on bifurcation-point calculations have been investigated and are reported in detail in Burroughs *et al.* (2001) and Salinger *et al.* (2002*b*). This includes comparisons of the bifurcation points using alternative discretization techniques (e.g. spectral methods) and comparisons with the SUPG stabilization disabled. We find that SUPG effects in our simulations are negligible. For example, at an aspect ratio of 0.125, the value of the Reynolds number of the pitchfork bifurcation point changed by 0.2 % when SUPG stabilization was disabled.

The mesh discretizations employed bilinear quadrilateral and trilinear hexahedral elements. The mesh density was adjusted to be higher near the jet inlets and in the stagnation region, and lower near the exits. A mesh refinement study is shown in the Appendix to demonstrate solution accuracy. For the planar rectangular jet geometry shown in figure 1(*a*), the finite element discretization utilized 6720 bilinear elements corresponding to 20 769 unknowns. The alternative model shown in figure 1(*b*) employed 16 640 bilinear elements corresponding to 50 913 unknowns. In the case of axisymmetric jets, the two-dimensional axisymmetric model corresponding to figure 2 was discretized using 3600 bilinear elements yielding 11 311 unknowns. The three-dimensional axisymmetric inlet model was solved using the mesh shown in figure 3 that contained 414 000 linear elements corresponding to 1 696 668 unknowns.

The discretzation of the governing equations yields a set of differential algebraic equations (DAEs) of the form

$$\boldsymbol{F}(\boldsymbol{x}, \dot{\boldsymbol{x}}, t, \mu) = \left\{ \begin{array}{c} F_P(\boldsymbol{x}, \mu) \\ F_{\boldsymbol{u}_1}(\boldsymbol{x}, \dot{\boldsymbol{x}}, t, \mu) \\ \vdots \\ F_{\boldsymbol{u}_i}(\boldsymbol{x}, \dot{\boldsymbol{x}}, t, \mu) \end{array} \right\} = \boldsymbol{0}. \tag{3.5}$$

$\boldsymbol{F}$ is defined as the set of residual equations resulting from the discretization of the PDEs, $\boldsymbol{x}$ is the dimensionless solution vector for all unknowns in the problem, t is the dimensionless time, $\dot{\boldsymbol{x}}$ is the dimensionless derivative of the solution vector with respect to time ($\partial x/\partial t$), μ is a parameter of interest in the bifurcation analysis, and i is the number of spatial dimensions in the model.

3.2. *Steady-state solver – Newton's method*

To obtain stationary points of the residual equations, we define a *steady-state* residual form of equation (3.5), $\boldsymbol{F}(\boldsymbol{x}, \mu) = 0$, by removing the time-dependent term in equation (2.2). In all subsequent continuation and bifurcation tracking routines, the steady-state residual equations are used. The time-dependent residual equations are used only when performing the stability analysis described in § 3.4 and for verifying that the Hopf bifurcation generated a periodic solution.

We solve the system of nonlinear residual equations using a fully coupled Newton–Krylov iterative solution method (described in Shadid, Tuminaro & Walker 1997; Shadid 1999). Applying Newton's method to equations (3.5) results in the following linear system that is solved at each iteration of the nonlinear sequence:

$$\boldsymbol{J}\Delta\boldsymbol{x} = -\boldsymbol{F}. \tag{3.6}$$

Here, $\boldsymbol{J}$ is the Jacobian matrix defined as $J_{ij} = \partial F_i/\partial x_j$, and $\Delta\boldsymbol{x}$ is the update to the latest estimate of the solution vector. To form the Jacobian of the system, equations (3.1) and (3.2) are linearized. In MPSalsa, the Jacobian is formed analytically and in parallel, and is stored in a distributed sparse format. The

resulting Newton equation is a fully coupled non-symmetric linear system, and is solved iteratively with domain-decompositon ILU preconditioned GMRES (Saad & Schultz 1986; Saad 1996). Successful termination of the nonlinear iterative process is based on a weighted root-mean-square norm (Brenan, Campbell & Petzold 1996; Byrne & Hindmarsh 1999):

$$C\sqrt{\frac{1}{N}\sum_{i=1}^{N}\left(\frac{\left(x_i^k - x_i^{k-1}\right)}{RTOL|x_i^{k-1}| + ATOL_i}\right)^2} < \epsilon, \tag{3.7}$$

where C is a constant, k is the current nonlinear iteration number, N is the number of unknowns in the system, $RTOL$ is the relative tolerance, $ATOL$ is the absolute tolerance (which can be a vector or constant value), and ϵ is the desired tolerance requested by the user. Additional details and parameter values can be found in the Appendix.

3.3. *Steady-state solution tracking: parameter continuation*

Once a steady-state solution has been obtained, the solution branch can be tracked as a function of a continuation parameter, μ. In this study the continuation parameters were the Reynolds number and aspect ratio. The Reynolds number is a scalar value that can be set during the continuation runs. The aspect ratio was set by algebraically adjusting the coordinate values of the original mesh that was created with an aspect ratio of 1.0.

The LOCA library (Salinger *et al.* 2002*a*, 2005) implements a variety of predictor–corrector algorithms for parameter continuation. In this study we use zero-order, Euler–Newton, and arc-length continuation algorithms. A full description of the algorithms can be found in Keller (1977). Zero-order continuation uses the solution from the previous continuation step as the initial guess for the next continuation step. The Euler–Newton algorithm computes the tangent at the previous continuation step, and extrapolates in that direction by the step length, to compute the initial guess for the next continuation step. In arc-length continuation, a monotonic arc-length variable s replaces the system parameter, μ, in the continuation stepper. The parameter μ is treated as an unknown and is calculated along with the solution vector. For arc-length continuation, an additional constraint equation G, which ensures that the next solution is a distance Δs from the previous solution, is solved simultaneously with the steady-state equations. The augmented set of nonlinear equations is

$$\boldsymbol{F}(\boldsymbol{x}, \mu) = 0, \tag{3.8a}$$

$$G(\boldsymbol{x}, \mu, s) = 0. \tag{3.8b}$$

The new system of equations is solved by using Newton's method again. In this case there are $m+1$ unknowns where m is the number of unknowns in the original steady-state problem and μ is the additional unknown.

3.4. *Stability analysis: eigenvalue and eigenvector calculations*

A linear stability analysis is used to identify bifurcation points along solution branches. This is accomplished through approximation of the leading eigenvalues of the linearized system using Arnoldi iteration (Arnoldi 1951), a technique first demonstrated by Christodoulou & Scriven (1988). We used the P_ARPACK software (Maschhoff & Sorensen 1996; Lehoucq, Sorensen & Yang 1998) in our simulations. Implementation details and a discussion of the spectral transformations can be found in Lehoucq & Salinger (2001, 1998), Salinger, Lehoucq & Romero (2001) and

Burroughs *et al.* (2004). A brief summary of the method follows. We note that for the two-dimensional meshes (planar and axisymmetric) the base flow is always perturbed within the computational domain. Perturbations in the third dimension were not analysed using the two-dimensional mesh domains. To identify three-dimensional disturbances we used the three-dimensional mesh.

A linearization of the time-dependent equations (equation (3.5)) about a steady-state solution leads to the following generalized eigenvalue problem:

$$\boldsymbol{J}\boldsymbol{w} = \boldsymbol{B}\boldsymbol{w}\lambda, \tag{3.9}$$

where $\boldsymbol{J}$ is the Jacobian matrix associated with the steady state, λ is the eigenvalue, and $\boldsymbol{w}$ is the eigenvector. $\boldsymbol{B}$, called the mass matrix, is the coefficient matrix of time-dependent terms, $\boldsymbol{B} = -\partial \boldsymbol{F}/\partial \dot{\boldsymbol{x}}$, evalutated at the steady state. Note that $\boldsymbol{B}$ is singular since the incompressible flow equations have no time derivatives for the pressure variable. Both λ and $\boldsymbol{w}$ can be complex.

The steady state is linearly stable if the real part of all eigenvalues is less than zero ($Re(\lambda) < 0$) for all eigenvalues of equation (3.9). Therefore, the rightmost eigenvalues (eigenvalues closest to the positive real half of the real-imaginary plane) of equation (3.9) are critical in determining the stability of a steady state.

To compute the rightmost eigenvalues, a generalized Cayley spectral transform (Meerbergen, Spence & Roose 1994; Lehoucq & Meergbergen 1998) is used to re-form the generalized eigenvalue problem into an ordinary eigenvalue problem (Lehoucq & Salinger 2001):

$$\boldsymbol{T}_s\boldsymbol{w} = (\boldsymbol{J} - \sigma_c\boldsymbol{B})^{-1}(\boldsymbol{J} - \mu_c\boldsymbol{B})\boldsymbol{w} = \nu\boldsymbol{w}, \quad \nu = \frac{\lambda - \mu_c}{\lambda - \sigma_c}. \tag{3.10}$$

Here σ_c is the pole and μ_c is the zero of the Cayley transform, and ν is the transformed eigenvalue. Selection of the Cayley parameters, σ_c and μ_c, is critical to map the correct set of eigenvalues (those with the largest real part) to the eigenvalues of the largest magnitude in the Cayley transform. The importance of this transform, when choosing $\lambda < \sigma_c < \mu_c$ for all λ as in Lehoucq & Salinger (2001), is that it maps the infinite negative eigenvalues generated by the continuity equation (resulting in a singular $\boldsymbol{B}$ from the incompressibility assumption) to a value of one. This makes the spectral condition number of the system smaller than other typical transformations such as the shift–invert spectral transformation. The resulting ordinary eigenvalue problem is solved using an implicitly restarted Arnoldi's method (Arnoldi 1951; Ruhe 1996; Meerbergen & Roose 1997) in P_ARPACK, each step of which requires an iterative linear solver to apply the inverse operator in equation (3.10).

3.5. *Parameter tracking of bifurcation points*

Once a bifurcation point is located and the eigenvalue and corresponding eigenvector near the bifurcation point have been calculated, the LOCA library can converge to the bifurcation point and track it as a function of a second parameter. Routines have been implemented in LOCA to track turning point, pitchfork, and Hopf bifurcations. The tracking algorithms continue in the parameter μ_1 (called the continuation parameter), and calculate the value of a second parameter, μ_2 (called the bifurcation parameter) such that the steady-state solution corresponds to the bifurcation point. In this way, two-parameter plots which map the transition between solution types can be generated.

To track a pitchfork bifurcation, the following system of equations is solved:

$$\boldsymbol{F}(\boldsymbol{x}, \mu_1, \mu_2) + \varepsilon\boldsymbol{\psi} = 0, \tag{3.11a}$$

$$\boldsymbol{\psi} \cdot \boldsymbol{x} = 0, \tag{3.11b}$$

$$\boldsymbol{J}\boldsymbol{n} = 0, \tag{3.11c}$$

$$\boldsymbol{\phi} \cdot \boldsymbol{n} - 1 = 0. \tag{3.11d}$$

In this system ε is a slack parameter representing the asymmetry in the system. If the numerical system is truly symmetric, then the algorithm will drive ε to zero, recovering the problem of interest. All meshes used in this study were symmetric. Equation (3.11*b*) requires the solution vector to be orthogonal to the antisymmetric vector $\boldsymbol{\psi}$ (forces the solution vector to be on the symmetric branch). There is a zero eigenvalue at a pitchfork bifurcation, so equations (3.11*c*) and (3.11*d*) are added. Equation (3.11*c*) makes the Jacobian singular if the null vector, $\boldsymbol{n}$, is non-zero. Equation (3.11*d*) forces $\boldsymbol{n}$ to be non-zero (normalizes the length of the null vector); $\boldsymbol{\phi}$ is a scaling vector that can be anything as long as $\boldsymbol{\phi} \cdot \boldsymbol{n} \neq 0$ at convergence, and usually we pick $\boldsymbol{\phi} = \boldsymbol{\psi}$. This system of equations expands the number of unknowns from m to $2m+2$. More details can be found in Salinger *et al.* (2005) on how these equations are solved without major code modifications.

To track a Hopf bifurcation, the following system of equations is solved:

$$\boldsymbol{F}(\boldsymbol{x}, \mu_1, \mu_2) = 0, \tag{3.12a}$$

$$\boldsymbol{J}\boldsymbol{y} + \omega \boldsymbol{B}\boldsymbol{z} = 0, \tag{3.12b}$$

$$\boldsymbol{J}\boldsymbol{z} - \omega \boldsymbol{B}\boldsymbol{y} = 0, \tag{3.12c}$$

$$\boldsymbol{\phi} \cdot \boldsymbol{y} - 1 = 0, \tag{3.12d}$$

$$\boldsymbol{\phi} \cdot \boldsymbol{z} = 0. \tag{3.12e}$$

Here $\boldsymbol{y}$ and $\boldsymbol{z}$ are the eigenvectors for the real and imaginary parts of the Hopf bifurcation ($\boldsymbol{w} = \boldsymbol{y} + \mathrm{i}\boldsymbol{z}$) and ω is the frequency of the Hopf bifurcation (the imaginary part of the eigenvaule of the Hopf bifurcation, or $\lambda = 0 + \mathrm{i}\omega$). $\boldsymbol{\phi}$ is an arbitrary scaling vector used to fix the amplitude and frequency of the eigenvectors. This system of equations expands the number of unknowns from m to $3m + 2$.

The flow code, solver, and stability calculations have been verified on a number of two-dimensional and three-dimensional flow problems (Burroughs *et al.* 2001; Salinger *et al.* 2002*b*).

4. Results and discussion

The results are divided into two sections based on the geometry of the jets. The two-dimensional flows resulting from the planar (rectangular) inlet jet geometries shown in figure 1 are discussed in § 4.1. The results of the simulations are compared to experimental data reported by Denshchikov *et al.* (1978, 1983). The analysis of stagnation flows formed by axisymmetric inlet jets is presented in § 4.2.

4.1. *Planar jets*

The work of Denshchikov *et al.* (1978, 1983) on flows resulting from planar counterflowing jets was carried out in a water-filled tank using two coplanar slit-shaped nozzles as inlets. The geometry used made the flow two-dimensional. We performed a parametric study on the structure and stability of the resulting flows using the two-dimensional model discussed in § 2. Four different flow regimes were identified depending on the values of Re and α.

The first flow regime corresponds to a single symmetric steady state. An example of this type of flow is depicted in figure 4 for a Reynolds number of 22.5 and aspect

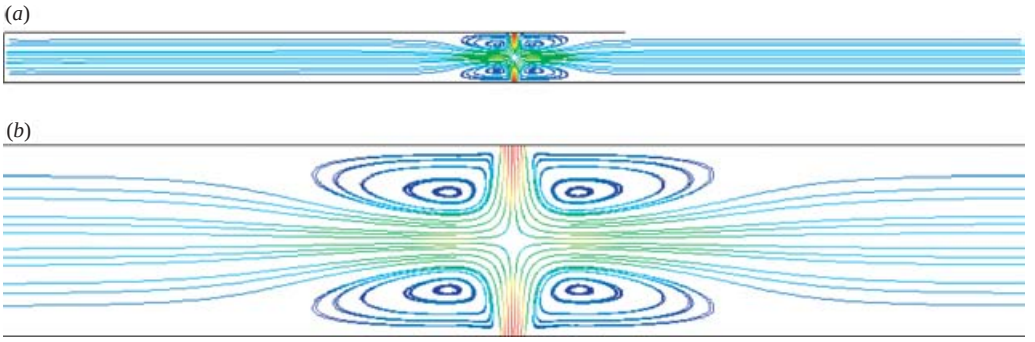

FIGURE 4. Streamlines for planar jets with $Re = 22.5$ and $\alpha = 0.125$. (*a*) Entire domain. (*b*) Close-up of the stagnation region. Colour code: red corresponds to largest velocity magnitude and blue to lowest.

ratio of 0.125. Figure 4(*a*) shows the entire computational domain while figure 4(*b*) shows a close-up of the stagnation region. The flow forms a well-defined stagnation pattern with four convectively driven flow recirculations on the sides of the inlet jets. Subsequent eigenvalue analysis indicated that the solution is stable. At low Re, this type of flow mode arises irrespective of the value of α.

At higher values of Re, transitions to two additional flow modes can occur. The corresponding bifurcation points of the transition were identified using eigenvalue analysis and parameter continuation techniques. For a fixed aspect ratio, a continuation from low to high Re values was performed. At each continuation step, the steady-state solution was obtained by using Newton's method. The leading eigenvalues were subsequently computed at the steady-state solution. At low Re the leading eigenvalue is real and has a negative real part corresponding to a stable steady state. Bifurcation points were identified when the real part of the leading eigenvalue crossed the imaginary axis. At mid to high aspect ratios this transition occurs through a pitchfork bifurcation with a single real eigenvalue crossing zero. At low aspect ratios on the other hand, the transition to a different flow mode occurs via a Hopf bifurcation arising when a pair of complex eigenvalues crosses the imaginary axis.

The second flow regime exists at large aspect ratios, for which the transition to a different flow mode occurs via a pitchfork bifurcation. This bifurcation is a breaking of symmetry about the midplane as noted in § 2.2. For a given aspect ratio, a critical Re can be identified above which there are three steady states instead of one; two stable and one unstable. To illustrate the transition to a flow regime with three possible steady states we fixed the aspect ratio at 0.125 and increased the value of Re from 22.5 (figure 4) to 27.5. In this case a pitchfork bifurcation point was identified at a critical $Re = 24.5$. Above this value, three steady states are present. The fluid streamlines for the three steady states at $Re = 27.5$ are shown in figure 5. The two leading eigenvalues are also listed for each case. Examination of the leading eigenvalue indicates that the flow patterns shown in figures 5(*a*) and 5(*c*) correspond to stable solutions. These solutions are mirror images of each other with respect to the midplane of the domain. The symmetric solution shown in figure 5(*b*) is unstable.

In the two asymmetric stable steady states, the stagnation point is located above or below the midplane, and there is also a pronounced reduction in the size of the recirculation areas towards the direction of the shift of the stagnation point. A

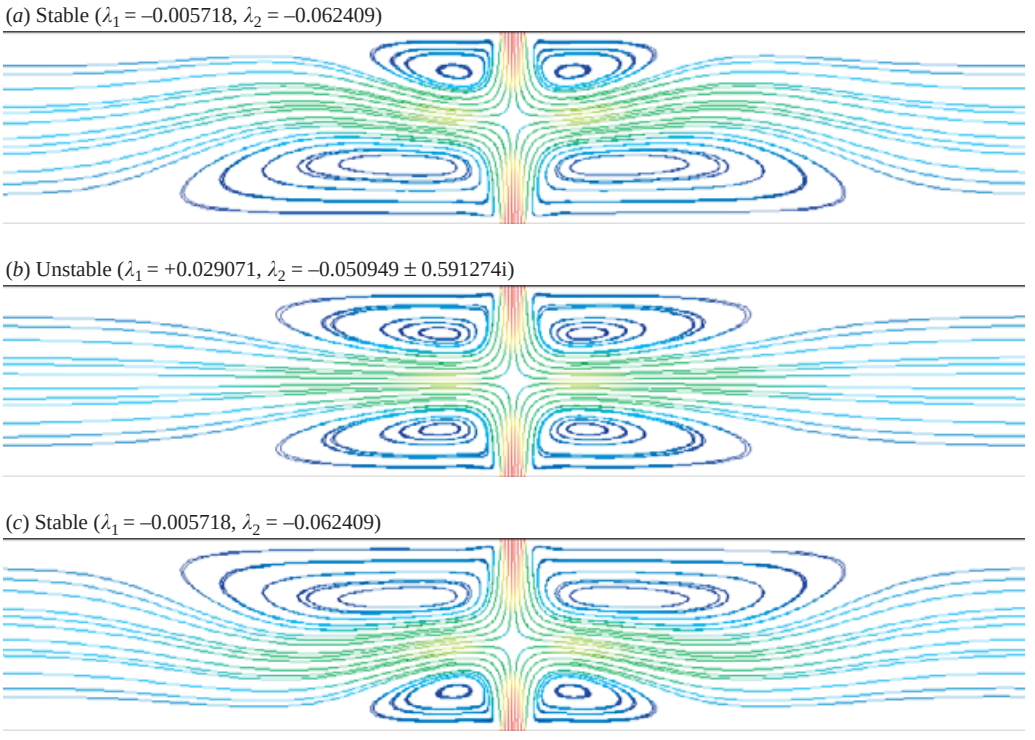

FIGURE 5. Streamlines for planar counterflowing jets with $\alpha = 0.125$ and $Re = 27.5$. Three steady states are possible: (*a*) stable asymmetric (upper branch), (*b*) unstable symmetric (middle branch) and (*c*) stable asymmetric (lower branch). The two rightmost (leading) eigenvalues are also shown for each steady state.

bifurcation diagram was computed to track the dependence of the location of the stagnation point on Re for a fixed $\alpha = 0.125$. The extent of the deflection of the stagnation point is used as a measure of the asymmetry of the solution. The diagram is shown in figure 6. A pitchfork bifurcation at $Re = 24.5$ marks the transition from a single steady state to three steady states for higher Re values. The two inlets correspond to values of 0.5 and -0.5 on the dimensionless deflection axis. The deflection of the stagnation point increases as the value of Re increases and can reach 50 % of the distance between the midpoint and the inlet.

At higher values of α the critical Re corresponding to the pitchfork bifurcation also increases. For example, the critical Re at $\alpha = 1.0$ is 872 while at $\alpha = 0.125$ the critical number is 24.5. At high aspect ratios, the jets are in close contact, requiring larger Reynolds numbers to generate the convective instability of the pitchfork bifurcation. High aspect ratios appears to stabilize the flow and also affects the asymmetric structure of the flow field. While deflections of the stagnation point can reach 50 % at smaller aspect ratios, the deflection of the stagnation point at $\alpha = 1.0$ is very small. Correspondingly, the size of the flow recirculation areas near the inlets is suppressed, as shown in figure 7.

The third flow regime, that arises for small aspect ratios, is characterized by oscillatory behaviour. The transition to oscillatory flow was found to occur via a Hopf bifurcation. This happens when the leading eigenvalue consists of a pair of complex conjugates whose initially negative real parts become zero before crossing the

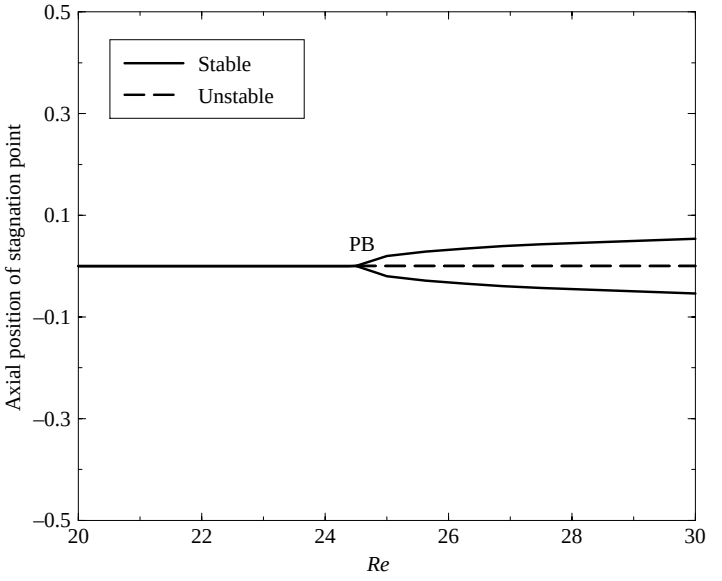

FIGURE 6. Bifurcation diagram for $\alpha = 0.125$. The position of the stagnation point along the y-axis is plotted *vs.* Re. The upper and lower jet inlets are located at 0.5 and -0.5, respectively. The point marked PB is the pitchfork bifurcation point. Solid lines correspond to stable steady states and the dashed line to unstable ones.

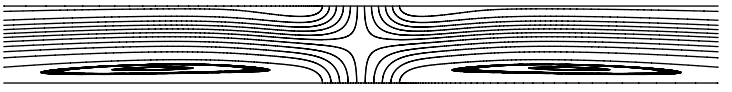

FIGURE 7. Streamlines corresponding to a stable solution (upper) branch for $Re = 1451$ and $\alpha = 1.0$. The deflection of the stagnation point is less than 1.0 % for this asymmetric solution.

imaginary axis as the value of a parameter is changed. Continuation with respect to Re was also used in this case to identify Hopf bifurcation points. For values of Re higher than the ones corresponding to the Hopf bifurcation point the symmetric steady state becomes unstable and a stable time-dependent (periodic) flow pattern appears. To study the periodic flow arising for Re higher than the critical one, a transient simulation was performed. Figure 8 shows snapshots of streamlines computed for $Re = 15$ and $\alpha = 0.1$ corresponding to roughly one period of the oscillatory flow pattern. In this case the jets deflect off each other and periodically swing left and right as time passes. This flow pattern agrees well with the reported 'deflecting jet oscillation' of Denshchikov *et al.* (1978, 1983).

To demonstrate the periodic character of the transient flow mode, the x-velocity component at a specific point in the domain is plotted as a function of dimensionless time in figure 9. In this case a period of approximately 12 dimensionless time units is observed in the transient simulations. Eigenvalue calculations about the unstable steady state predict a period of 11.98 dimensionless time units.

Once the bifurcation points were located, tracking algorithms (equations (3.11) and (3.12)) in conjunction with parameter continuation were used to directly calculate entire branches of bifurcation points. One parameter was used as the continuation parameter, and the second parameter was directly calculated such that the steady-state solution corresponds to the bifurcation point. A two-parameter plot of the Reynolds

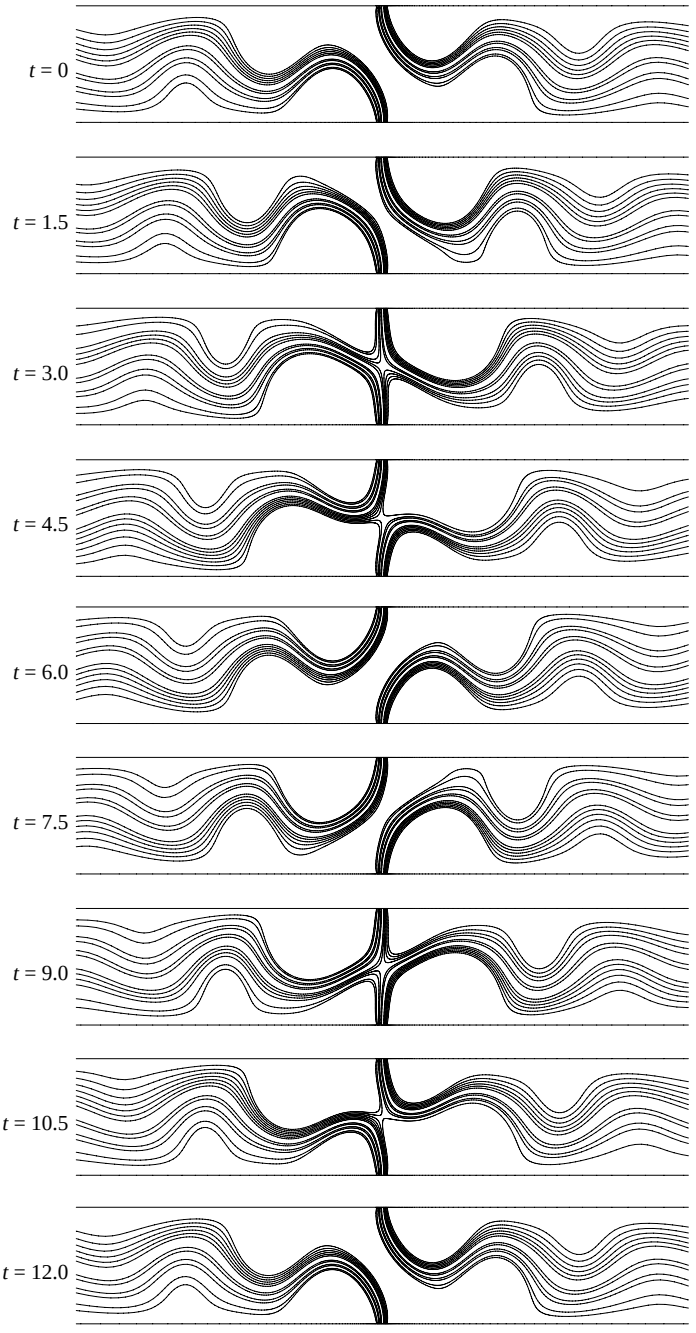

FIGURE 8. Streamline snapshots demonstrating oscillatory behaviour (deflecting jet oscillation) in a planar counterflowing jet obtained by a transient simulation in dimensionless time at $Re = 15$ and $\alpha = 0.1$. The dimensionless period of the oscillation is approximately 12.

number as a function of aspect ratio was generated based on the tracking algorithm data and is shown in figure 10. The curves denote the bifurcation points computed on the stable flow branches. The branches separate the behaviour of counterflowing jets into three different flow modes or regions: (I) the single stable steady state,

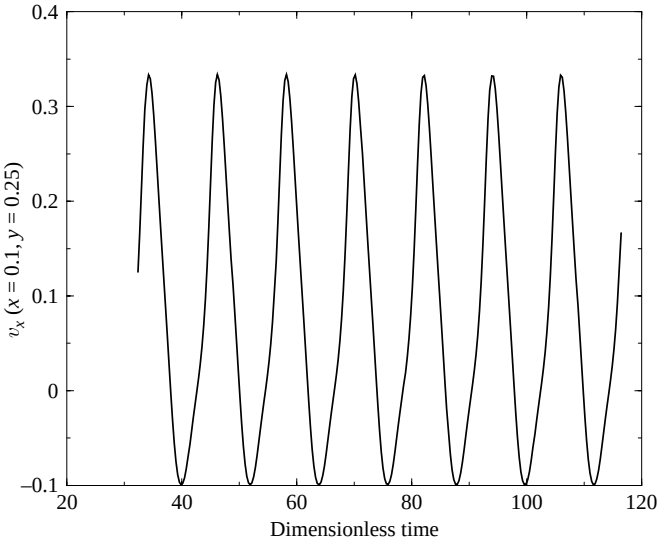

FIGURE 9. Plot of the dimensionless x-component of velocity at $x = 0.1$ and $y = 0.25$ for the conditions corresponding to figure 8.

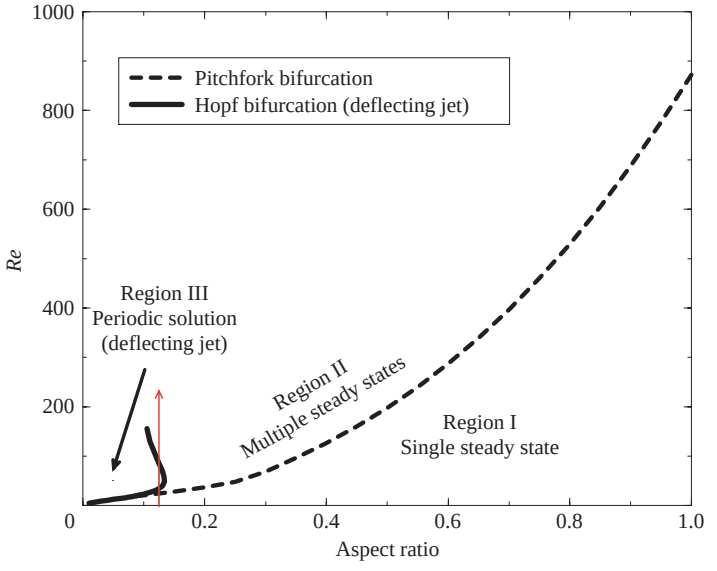

FIGURE 10. Map of the parameter space indicating different flow regimes arising in planar counterflowing jets. The red arrow indicates the continuation path used to construct the bifurcation diagram shown in figure 11.

(II) multiple steady states, and (III) time-dependent periodic flow with deflecting jet oscillations. An interesting point is the intersection of the pitchfork and Hopf bifurcation curves at a Reynolds number of 11.2 and an aspect ratio of 0.075. A real eigenvalue and a complex-conjugate pair of eigenvalues all cross the imaginary axis at the same time. To the left of this point, the Hopf bifurcation occurs on a stable symmetric branch, but to the right of this point the Hopf bifurcation occurs

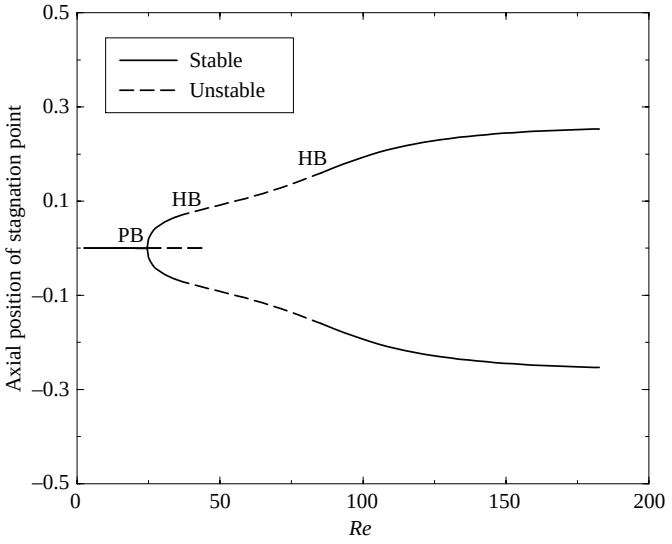

FIGURE 11. Bifurcation diagram for $\alpha = 0.125$ following the path of increasing Re indicated by the red arrow in figure 10. PB, pitchfork bifurcation; HB, Hopf bifurcation.

on all three branches. In figure 10 only the Hopf bifurcations occurring on the stable asymmetric branches are shown.

An important feature of the Hopf bifurcation branch in figure 10 is its shape. As the aspect ratio increases, this branch turns back towards smaller aspect ratios. As a result, there is a maximum aspect ratio after which the deflecting jet oscillation cannot occur no matter what the value of Re is. This feature can generate a complex behaviour. We demonstrate this by performing a continuation in the Reynolds number at a fixed aspect ratio of 0.125. The arrow in figure 10 shows the path taken through parameter space to compute the bifurcation diagram in figure 11. Starting at $Re = 1.0$ the flow mode corresponds to a single stable steady state. If we increase the value of Re we encounter a pitchfork bifurcation and a transition to one of two stable asymmetric flow patterns (with the symmetric flow corresponding to the original branch that becomes unstable). Further increase in Re leads to a Hopf bifurcation and the stable asymmetric steady state becomes oscillatory. At even higher values of Re the oscillatory behaviour disappears and the flow pattern reverts back to one of two stable asymmetric steady states. The coexisting oscillatory solutions are not computed and are not plotted in figure 11. Only the unstable steady state is plotted for the Hopf bifurcation.

Knowledge of the complex flow phenomena arising along the path traced in figure 11 by changing a single parameter (Re) is critical for applications utilizing counterflowing jets. The observed behaviour of an experimental system following such a path can be very confusing, unless a fundamental understanding of the possible stable flow patterns, as presented above, is available. In an experimental setup corresponding to figure 11 ($\alpha = 0.125$) and utilizing various flow rates (different values of Re), the flow pattern can be stable and symmetric at low Re, stable and asymmetric for Re beyond the PB point, oscillatory beyond the HB point, and stable and asymmetric again at higher values of Re. In experimental investigations the root cause of such a plethora of complex flow patterns could be erroneously sought in equipment design and instrument calibration issues and not in the underlying physics.

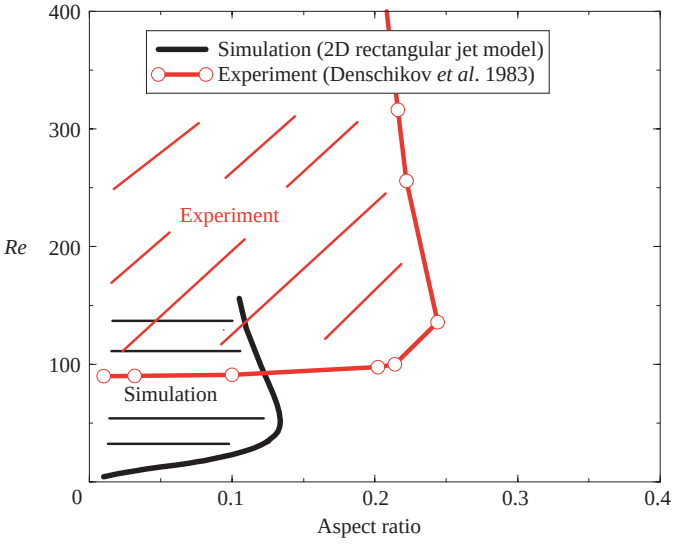

FIGURE 12. Map of the parameter space comparing the predictions of the simulations with the experiments of Denshchikov *et al.* (1978, 1983) on the onset of deflecting jet oscillations in planar counterflowing jets.

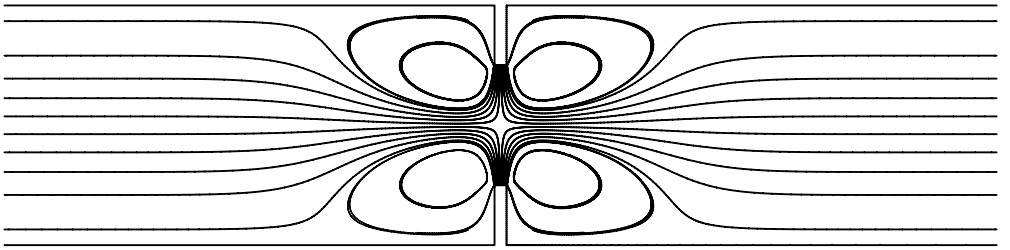

FIGURE 13. Streamline plot for the alternative planar counterflow jet geometry of figure 1(*b*) for $Re = 50$ and $\alpha = 0.1$.

A comparison between the predictions of our simulations and the experimental results reported by Denshchikov *et al.* (1978, 1983) is shown in figure 12. The experimental data and the simulation results show strikingly similar trends in terms of the shape and location of the oscillatory flow region in parameter space. The agreement in this case is only qualitative. The reasons can be sought for differences between the simulations and the experiments in the geometry of the domain as well as in operating and boundary conditions. The experimental set-up did not include horizontal retaining walls for the exit flow, but employed an open geometry with the jets expanding into an 'infinite' fluid after colliding with each other. Furthermore, no error bars or resolution limits were reported in the experimental study that places the onset of oscillatory flow at $Re = 90$ and persisting at aspect ratios as high as 0.24. For comparison, the model predicts the onset of oscillatory flow at $Re = 4$ and persisting at aspect ratios as high as 0.13.

Simulations were also performed using the alternative planar jet arrangement shown in figure 1(*b*) in an effort to resolve the above discrepancies between theory and experiments. Figure 13 shows the predicted streamlines from a typical simulation utilizing the new geometry. The simulations based on the alternative geometry resulted

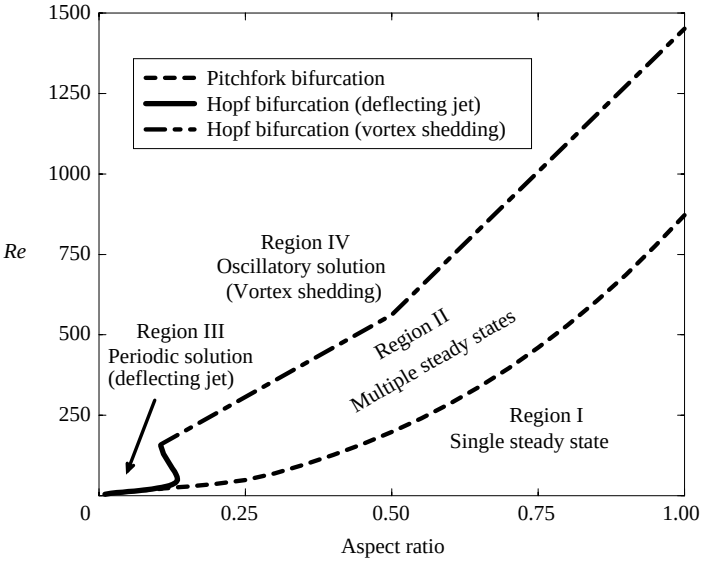

FIGURE 14. A more complete map of the parameter space indicating the regions corresponding to the four different flow regimes that may arise in laminar planar counterflowing jets.

in essentially the same Hopf bifurcation curve as the one shown in figure 12. We conclude that the discrepancies were not the result of the exit wall confinement although conditions inside the experimental tank could not be ruled out in general.

Finally, a fourth flow regime that corresponds to oscillatory flow with vortex shedding was observed at high values of *Re*, irrespective of the aspect ratio. The transition to this flow mode is caused by Hopf bifurcations leading to periodic flows. The leading eigenmodes typically correspond to downstream recirculations away from the stagnation flow region. There is no single mode that causes this type of instability and multiple bifurcating modes were located at different aspect ratios. Continuation runs in *Re* revealed multiple Hopf bifurcations crossing the imaginary axis in rapid succession at high *Re*, suggesting a transition to chaotic flows. Figure 14 shows a rough outline of this region based on three data points. This curve is not the result of tracking a single mode but was generated using independent eigenvalue calculations. This was done because the eigenmode that destabilized the flows changed with aspect ratio. More details on the vortex shedding region can be found in Pawlowski (2000).

4.2. *Axisymmetric jets*

The flow patterns obtained from simulations of axisymmetric jets, using the three-dimensional axisymmetric (and hence two-dimensional) domain (figure 2) and the fully three-dimensional domain (figure 3), are discussed in this section. The analysis focused on identifying values of the parameters for which transitions occur to flow patterns that are different from the expected single and symmetric stable steady state. The bifurcation analysis on the three-dimensional axisymmetric model was performed following the same procedures used for the analysis of planar counterflowing jets. For *Re* between 1 and 2100 and aspect ratios between 0.05 and 1.5, no Hopf bifurcation points were found, thus eliminating the possibility of oscillatory flow patterns (deflecting jet oscillations and vortex shedding) like the ones predicted for planar jets. The only type of flow transition found for axisymmetric jets corresponded to a pitchfork bifurcation that leads to three steady states, analogous to those discussed in

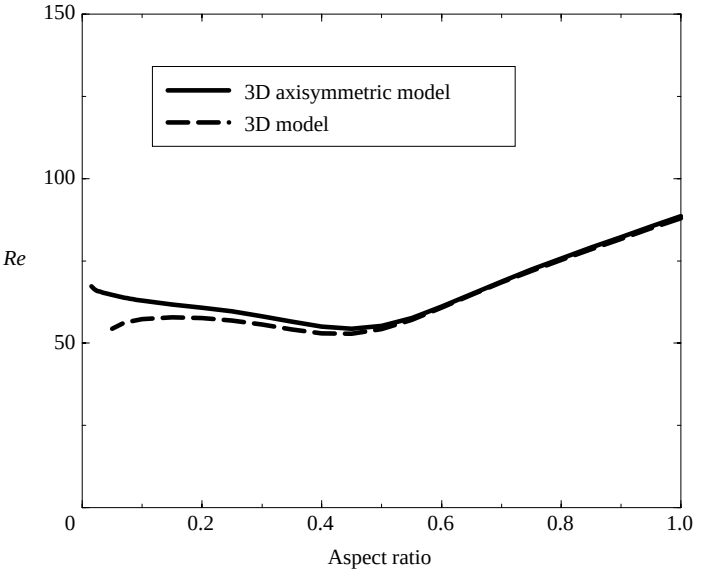

FIGURE 15. Parameter plot for axisymmetric counterflowing jet inlets. Lines represent pitchfork bifurcation points located on stable solution branches.

the previous section. Again, continuation of the pitchfork bifurcation delineates the two different flow regimes in parameter space. The result is shown by the solid line in figure 15. At low Re, the flow is dominated by viscous effects and a single symmetric steady state is obtained. The transition to three steady states occurs for Re higher than about 60 for aspect ratios up to 0.5. For higher aspect ratios (i.e. for small jet separations) the critical value of Re required to force the transition increases almost linearly with α, following the formula $Re_{cr} = 60(\alpha + 0.5)$.

The stability of these axisymmetric solutions to three-dimensional disturbances was investigated. Since we do not have the capability of studying three-dimensional disturbances to three-dimensional axisymmetric flows, a full three-dimensional model (figure 3) was constructed to investigate the annular disturbances. In particular, we conjectured that a three-dimensional analogue to the deflecting jet oscillations (e.g. swirling jets) in planar jets would exist. No three-dimensional modes overtook the axisymmetric mode in the range of parameter values studied here. As shown by the dashed line in figure 15 only the pitchfork bifurcation was detected. There is a small difference in the predictions of the three-dimensional axisymmetric and full three-dimensional models at low aspect ratios (large jet separations) attributed to numerical artifacts that are related to the distortion of the three-dimensional mesh. The mesh was created for $\alpha = 1.0$ and was algebraically deformed to fit the other aspect ratios. At aspect ratios higher than 0.5 the predictions between the two models are almost identical. A single calculation with 10 million unknowns was performed (on 160 processors) at $\alpha = 1.0$ to verify that the mesh resolution was adequate. With this level of resolution, the prediction of the bifurcation point for the two models agreed to three digits.

The suppression of oscillatory flow behaviour in the three-dimensional axisymmetric jet flows, compared to the two-dimensional planar flows, must be related to the divergence and corresponding deceleration of the flow as it travels radially. No breaking of the rotational symmetry, necessary for realization of oscillatory flows,

was observed for the conditions studied here. Furthermore, the deflection of the stagnation point from the origin along the z-axis is less pronounced in axisymmetric opposed jets when compared to planar jets. The maximum deflection occurs at the smallest aspect ratio that we studied ($\alpha = 0.05$) and was computed to be about 13.5 % of the distance between the centre of the reactor and the jet inlet for $Re = 78$.

The asymmetric flow patterns observed by Rolon *et al.* (1991) can be attributed to the flow mode obtained for values of Re higher than the critical ones corresponding to the pitchfork bifurcation. The jets used in their experiments were more complicated than the ones used in this study, but the observed behaviour is identical to the flows demonstrated with our analysis.

5. Conclusions

A fundamental study of the structure and stability of laminar flow patterns in planar and axisymmetric counterflowing jets of an isothermal incompressible Newtonian fluid was performed. The different flow regimes that may arise were identified and mapped on a two-dimensional parameter space formed by the Reynolds number (Re) and a geometric aspect ratio α (jet characteristic dimension/jet separation). These calculations were enabled by linear stability and bifurcation tracking algorithms for large-scale applications.

Stagnation flows formed by identical counterflowing planar jets exhibited complex behaviour classified into four distinct flow modes corresponding to: (*a*) a symmetric single steady state, (*b*) three steady states (two stable asymmetric ones and an unstable symmetric one), (*c*) a 'deflecting jet' oscillatory flow, (*d*) time-dependent chaotic flow with vortex shedding.

Stagnation flows formed by identical axisymmetric jets exhibited a transition from a single symmetric steady state to three steady states (two stable asymmetric ones and an unstable symmetric one). The three steady states are obtained under the following conditions: (i) $Re > 60$ for α less than or equal to 0.5 or (ii) $Re > 60(\alpha + 0.5)$ for α greater than 0.5 (and up to 1.0). No oscillatory instabilities were found in this geometry.

The ability to predict the various flow modes arising from counterflowing jets is crucial for the effective use of these flows in practical applications. The most important finding of our study is the existence of stable asymmetric and/or time-dependent flow patterns when the macroscopic operating conditions (geometry and inlet flow rates) are symmetric.

We thank David Day and Mike Heroux for their help in implementing the Komplex Library for Hopf Bifurcation tracking. We would also like to thank Rich Lehoucq for many helpful discussions about eigenvalue calculations. Funding for this project was provided by the National Science Foundation (CTS) and the Advanced Strategic Computing Initiative (ASCI). We also thank two anonymous reviewers for their constructive criticism of the manuscript. Sandia is a multiprogram laboratory operated by Sandia Corporation, a Lockheed Martin Company, for the United States Department of Energy under contract DE-AC04-94AL85000.

Appendix. Numerical solution details

The solution of the linear system $\boldsymbol{J}\Delta\boldsymbol{x} = -\boldsymbol{F}$ was achieved using a domain decomposition ILUT preconditioned GMRES algorithm implemented in the Aztec software

Levels of refinement	Nodes	Unknowns	Re_{pf}	% Error
0	6321	18 963	24.39	2.6
1	24 905	74 715	24.80	0.96
2	98 865	296 595	24.98	0.23
3	393 953	1 181 859	25.04	–

TABLE 1. Mesh dependence study for $\alpha = 0.125$ using three levels of mesh refinement. The computed values of Re_{pf} correspond to the Reynolds number of the pitchfork bifurcation point. The % Error is the error in the Re_{pf} compared to the value from the mesh with the highest level of refinement.

(Hutchinson *et al.* 1995). The iteration sequence was terminated when the following criterion was met:

$$||\boldsymbol{F}(\boldsymbol{x}_k) + \boldsymbol{J}(\boldsymbol{x}_k)\Delta\boldsymbol{x}|| \leqslant \eta_k ||\boldsymbol{F}(\boldsymbol{x}_k)||, \tag{A 1}$$

where η_k is a user-specified tolerance for Newton iteration k. In our simulations, η_k was set to a constant value of 1.0×10^{-4} when solving for a single steady state and tightened to 1.0×10^{-6} when using a bifurcation tracking or stability analysis algorithm. For steady-state solutions, the Krylov subspace was set to a maximum of 400. The algorithm typically required between 30 and 150 GMRES iterations to converge the linear system, depending on the Reynolds number. For the bifurcation tracking algorithms, the Jacobian matrix was near singular and the Krylov subspace was extended to a maximum of 800 iterations to achieve convergence. Three levels of overlap were used.

The nonlinear iteration sequence was terminated when the criterion described in equation (3.7) was met. When solving for the steady state, the following values were used: $C = 1.0$, $RTOL = 1.0 \times 10^{-5}$, $ATOL = 1.0 \times 10^{-8}$, and $\kappa = 1.0$. The $RTOL$ value was relaxed to 1.0×10^{-2} for the null vector component during the bifurcation tracking runs due to the difficulty in resolving the null vectors in equations (3.11) and (3.12). This change did not have a significant impact on the results. For example, at $\alpha = 0.125$ the value of the Reynolds number at the pitchfork bifurcation point changed only in the fourth digit of accuracy when the tolerance was dropped from 1.0×10^{-5} to 1.0×10^{-2}.

A study of the mesh dependence was performed to determine the accuracy at an aspect ratio of 0.125. Table 1 shows the results for the critical Re obtained on four meshes: an initial coarse mesh and three meshes at increasing levels of refinement. Each level of refinement represents a bisection of each edge in the mesh so that each two-dimensional quadrilateral element becomes four elements at the next level of refinement. The predicted value for the pitchfork bifurcation using the initial (more coarse) mesh differs by only 2.5 % from the value predicted using the highest resolution; thus we consider the initial resolution to be adequate.

REFERENCES

ARNOLDI, W. E. 1951 The principle of minimized iterations in the solution of the matrix eigenvalue problem. *Q. Appl. Maths* **9**, 17–29.

BIRD, R. B., STEWART, W. E. & LIGHTFOOT, E. N. 1960 *Transport Phenomena*. Wiley.

BIXLER, N. E. & SCRIVEN, L. E. 1987 Downstream development of three-dimensional viscocapillary film flow. *Ind. Engng Chem. Res.* **26**, 475–483.

BRENAN, K. E., CAMPBELL, S. L. & PETZOLD, L. R. 1996 *Numerical Solution of Initial-Value Problems in Differential-Algebraic Equations*. Classics in Applied Mathematics, vol. 14. SIAM.

Burroughs, E. A., Lehoucq, R. B., Romero, L. A. & Salinger, A. G. 2004 Linear stability of flow in a differentially heated cavity via large-scale eigenvalue calculations. *Intl J. Numer. Meth. Heat Fluid Flow* **14**, 803–822.

Burroughs, E. A., Romero, L. A., Lehoucq, R. B. & Salinger, A. G. 2001 Large scale eigenvalue calculations for computing the stability of buoyancy driven flows. *Tech. Rep.* SAND2001-0113. Sandia National Laboratories, Albuquerque.

Byrne, G. D. & Hindmarsh, A. C. 1999 Pvode, an ode solver for parallel computers. *Tech. Rep.* UCRL-JC-132361, Rev. 1. Center for Applied Scientific Computing (CASC), Lawrence Livermore National Lab.

Christodoulou, K. N. & Scriven, L. E. 1988 Finding leading modes of a viscous free surface flow: an asymmetric generalized eigenproblem. *J. Sci. Comput.* **3**, 355–406.

Coyle, D. J., Macosko, C. W. & Scriven, L. E. 1990 Stability of symmetrical film-splitting between counter-rotating cylinders. *J. Fluid Mech.* **216**, 437–458.

Denshchikov, V. A., Kontratev, V. N. & Romashev, A. N. 1978 Interaction between two opposed jets. *Fluid Dyna.* **6**, 924–926.

Denshchikov, V. A., Kontratev, V. N., Romashev, A. N. & Chubarov, V. M. 1983 Auto-oscillations of planar colliding jets. *Fluid Dyna.* **3**, 460–462.

Fotache, C. G., Kreutz, T. G. & Law, C. K. 1997 Ignition of counterflowing methane versus heated air under reduced and elevated pressures. *Combust. Flame* **108**, 442–470.

Grimes, R. Y., Pulido, G. A., Levine, R. A. & Yoganathan, A. P. 1996 Quasisteady behavior of pulsatile, confined, counterflowing jets: Implications for the assessment of mitral and tricuspid regurgitation. *J. Biomech. Engng* **118**, 498–505.

Gupta, V., Safvi, S. A. & Mountziaris, T. J. 1996 Gas-phase decomposition kinetics in a wall-less environment using a counterflow jet reactor: design and feasibility studies. *Ind. Engng Chem. Res.* **35**, 3248–3255.

Hughes, T., Franca, L. & Balestra, M. 1986 A new finite element formulation for computational fluid dynamics: V. Circumventing the Babuska-Brezzi condition: A stable Petrov-Galerkin formulation of the Stokes problem accommodating equal-order interpolations. *Comput. Meth. Appl. Mech. Engng* **59**, 85–99.

Hutchinson, S. A., Shadid, J. N. & Tuminaro, R. S. 1995 Aztec user's guide: Version 1.0. *Tech. Rep.* SAND95-1559. Sandia National Laboratories, Albuquerque.

Keller, H. B. 1977 Numerical solution of bifurcation and nonlinear eigenvalue problems. In *Applications of Bifurcation Theory* (ed. P. H. Rabinowitz), pp. 159–384. Academic.

Kistler, S. F. & Scriven, L. E. 1994 Teapot effect: Sheet-forming flows with deflection, wetting and hysteresis. *J. Fluid Mech.* **263**, 19–62.

Leclerc, A. 1950 Deviation d'un jet liquide par une plaque normale a son axe. *La Houille Blanche* **6**, 3.

Lehoucq, R. & Salinger, A. 2001 Large-scale eigenvalue calculations for stability analysis of steady flows on massively parallel computers. *Intl J. Number. Meth. Fluids* **36**, 309–327.

Lehoucq, R. B. & Meergbergen, K. 1998 Using generalized Cayley transformations within an inexact rational Krylov sequence method. *SIAM J. Matrix Anal. Appl.* **20**, 131–148.

Lehoucq, R. B. & Salinger, A. G. 1998 Massively parallel linear stability analysis with P_ARPACK for 3D fluid flow modeled with MPSalsa. *Lect. Notes Comput. Sci.* **1541**, 286–295.

Lehoucq, R. B., Sorensen, D. C. & Yang, C. 1998 *ARPACK USERS GUIDE: Solutions of Large Scale Eigenvalue Problems*. Philadelphia, PA: SIAM.

Liñán, A. 1974 The asymptotic structure of counterflow diffusion flames for large activation energies. *Acta Astronautica* **1**, 1007–1039.

Maschhoff, K. J. & Sorensen, D. C. 1996 P_ARPACK: An efficient portable large scale eigenvalue package for distributed memory parallel architectures. In *Applied Parallel Computing in Industrial Problems and Optimization* (ed. J. Wasniewski, J. Dongarra, K. Madsen & D. Oleson). Lecture Notes in Computer Science, vol. 1184. Springer.

Meerbergen, K. & Roose, D. 1997 The restarted Arnoldi method applied to iterative linear system solvers for the computation of rightmost eigenvalues. *SIAM J. Matrix Anal. Appl.* **18**, 1–20.

Meerbergen, K., Spence, A. & Roose, D. 1994 Shift-invert and Cayley transforms for the detection of rightmost eigenvalues of nonsymmetric matricies. *BIT* **34**, 409–423.

Pawlowski, R. P. 2000 Numerical studies of complex reacting flows. PhD thesis, State University of New York at Buffalo.

Puri, I. K., Seshadri, K., Smooke, M. D. & Keyes, D. E. 1987 A comparison between numerical calculations and experimental measurements of the structure of a counterflow methane-air diffusion flame. *Combust. Sci. Tech.* **56**, 1–22.

Rolon, J. C., Veynante, D. & Martin, J. P. 1991 Counterjet stagnation flows. *Exps. Fluids* **11**, 313–324.

Ruhe, A. 1996 Computing nonlinear eigenvalues with spectral transformation Arnoldi. *ZAMM Z. Angew. Math. Mech.* **76** (S2), 17–20.

Saad, Y. 1996 *Iterative Methods for Sparse Linear Systems*. Boston, MA: PWS.

Saad, Y. & Schultz, M. H. 1986 GMRES: A generalized minimal residual algorithm for solving nonsymmetric linear systems. *SIAM J. Sci. Statist. Comput.* **7**, 856–869.

Safvi, S. A. 1995 Studies of thermal decomposition reactions in a counterflow jet reactor and growth of gallium arsenide films by metalorganic chemical vapor deposition. PhD thesis, State University of New York at Buffalo.

Safvi, S. A. & Mountziaris, T. J. 1993 Gas-phase decomposition kinetics of MOVPE precursors in a counterflow jet reactor. In *Chemical Perspectives of Microelectronic Materials III*, *Mater. Res. Soc. Symp. Proc.*, vol. 282, pp. 157–162. Materials Research Society.

Safvi, S. A. & Mountziaris, T. J. 1994 A new reactor for purely homogeneous kinetic studies of endothermic reactions. *AIChE J.* **40**, 1535–1548.

Salinger, A. G., Bou-Rabee, N. M., Pawlowski, R. P., Wilkes, E. D., Burroughs, E. A., Lehoucq, R. B. & Romero, L. A. 2002*a* LOCA 1.0 A library of continuation algorithms: Theroy and implementation manual. *Tech. Rep.* SAND2002-0396. Sandia National Laboratories, Albuquerque.

Salinger, A. G., Burroughs, E. A., Pawlowski, R. P., Phipps, E. T. & Romero, L. A. 2005 Bifurcation tracking algorithms and software for large scale applications. *Intl J. Bifurcat. Chaos* **15**, 1015–1032.

Salinger, A. G., Devine, K. D., Hennigan, G. L., Moffat, H. K., Hutchinson, S. A. & Shadid, J. N. 1996 MPSalsa: A finite element computer program for reacting flow problems – part II user's guide. *Tech. Rep.* SAND96-2331. Sandia National Laboratories, Albuquerque.

Salinger, A. G., Lehoucq, R. B., Pawlowski, R. P. & Shadid, J. N. 2002*b* Computational bifurcation and stability studies of the 8:1 thermal cavity problem. *Intl J. Numer. Meth. Fluids* **20**, 1059–1073.

Salinger, A. G., Lehoucq, R. B. & Romero, L. 2001 Stability analysis of large-scale incompressible flow calculations on massively parallel computers. *Comput. Fluid Dyn. J.* **9**, 529–534.

Sarigiannis, D., Peck, J., Kioseoglou, G., Petrou, A. & Mountziaris, T. J. 2002 Characterization of vapor-phase-grown ZnSe nanoparticles. *Appl. Phys. Lett.* **80**, 4024–4026.

Shadid, J. N. 1999 A fully-coupled Newton-Krylov solution method for parallel unstructured finite element fluid flow, heat and mass transfer simulations. *Intl J. Comput. Fluid Dyna.* **12**, 199.

Shadid, J. N., Moffatt, H. K., Hutchinson, S. A., Hennigan, G. L., Devine, K. D. & Salinger, A. G. 1996 MPSalsa: A finite element computer program for reacting flow problems – Part I theoretical development. *Tech. Rep.* SAND95-2752. Sandia National Laboratories, Albuquerque.

Shadid, J. N., Tuminaro, R. S. & Walker, H. F. 1997 An inexact Newton method for fully-coupled solution of the Navier–Stokes equations with heat and mass transport. *J. Comput. Phys.* **137**, 155–185.

Tamir, A. 1994 *Impinging Stream Reactors, Fundamentals and Applications*. Transport Processes in Engineering 7. Elsevier.

Tezduyar, T. E. 1992 Stabilized finite element formulations for incompressible flow computations. *Adv. Appl. Mech.* **28**, 1.

Vlachos, D. G., Schmidt, L. D. & Aris, R. 1993 Ignition and extinction of flames near surfaces: Combustion of H_2 in air. *Combust. Flame* **95**, 313–335.

Wood, P., Hrymak, A., Yeo, R., Johnson, D. & Tyagi, A. 1991 Experimental and computational studies of the fluid mechanics in an opposed jet mixing head. *Phys. Fluids* A **3**, 1362–1368.

Zachariah, M. R. & Semerjian, H. G. 1989 Simulation of ceramic particle formation: comparison with in-situ measurements. *AIChE J.* **35**, 2003–2012.

Zhao, J. & Isaac, K. M. 1997 Influence of geometry and heat release on counterflow diffusion flames: A Navier-Stokes model. *Intl J. Comput. Fluid Mech.* **8**, 287–298.